Interleaved Critical Current Mode Boost PFC Converter With Coupled Inductor

Fei Yang, *Student Member, IEEE*, Xinbo Ruan, *Senior Member, IEEE*, Yang Yang, and Zhihong Ye, *Member, IEEE*

***Abstract*—Interleaved critical current mode (CRM) boost power factor correction (PFC) converter is widely employed recently for its high power density. In order to further reduce the volume and the copper usage of the magnetic components, two-phase interleaved CRM boost PFC converter with a coupled inductor is analyzed in this paper. The coupling effects on the input current, the inductor current, the switching frequency and the flux linkage are analyzed separately. If the self-inductances and the magnetic core are the same for both coupled and noncoupled inductors, the number of winding turns of coupled inductor is fewer than that of the noncoupled inductor, which implies a lower cost. Although the input current ripple increases a little since coupling, a reduction in the total volume of magnetic components, including the electromagnetic interference filter and the coupled inductor, is possible if the coupling coefficient is made reasonable.**

***Index Terms*—Boost converter, coupled inductor, critical current mode (CRM), interleaving, power factor correction (PFC).**

I. Introduction

THE boost converter operating in continuous current mode (CCM) is widely used in power factor correction (PFC) for its high power factor (PF) and low inductor current ripple. However, the power switch is hard-switching, and the boost inductor is relatively large. Critical current mode (CRM) boost PFC converter achieves zero-current turn-on for the power switch and zero-current turn-off for the diode, avoiding the reverse recovery problems, and the input PF is nearly unity. Although, the inductor is small, the input current is relatively large and it requires a large electromagnetic interference (EMI) filter. Therefore, CRM is only suitable for low power applications [1]. When multiple converters paralleled or interleaved, the output power can be extended without sacrificing the advantages of the single-phase converter, and it can also reduce the input and output current ripples [2]–[6], leading to a smaller EMI filter. Therefore, with the development of the control strategies [7]–[10] and the promotion of high power density and efficiency power supply, the interleaved CRM boost PFC converter is widely used recently.

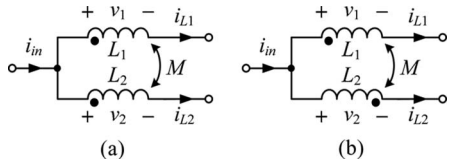

Fig. 1. Coupled inductor when (a) directly coupled and (b) inversely coupled.

The concept of coupled inductor has been applied successfully in the interleaved voltage regular modules for the improvement of the transient response and the inductor current ripple [11]–[13]. Meanwhile, coupled inductor employed in the interleaved boost PFC converter also exhibits improved performance, such as increased efficiency, smaller size, and reduced EMI filter [14]–[20].

Since the former researches are mainly focused on the coupled inductor effects on the interleaved boost PFC converter in CCM, the objective of this paper is to investigate the characteristics of interleaved CRM boost PFC converter with the boost inductors coupled. First, the switching frequency and the inductor current are deduced. Second, such coupling effects on the converter as the minimum switching frequency, the flux linkage in the magnetic core legs, and the input current are presented. Third, the proper coupling coefficient is discussed. Finally, a 300-W prototype is built, and the experimental results are provided.

II. Interleaved CRM Boost PFC Converter With the Coupled Inductor

A. Coupled Inductor

Two inductors can be coupled directly or inversely, as shown in Fig. 1. The circuit equation is

$$\begin{cases} v_1 = L_1 \dfrac{di_{L1}}{dt} \pm M \dfrac{di_{L2}}{dt} & \text{(1a)} \\ v_2 = L_2 \dfrac{di_{L2}}{dt} \pm M \dfrac{di_{L1}}{dt} & \text{(1b)} \end{cases}$$

where v_1 and v_2 are the voltages applied on the two windings, i_{L1} and i_{L2} are the inductor currents, L_1 and L_2 are the self-inductance of two windings, M is the mutual inductance. The sign before M is "+" or "−" when the inductors are coupled directly or inversely, respectively.

If $i_{L1} = i_{L2}$, (1a) can be written as $v_1 = (L_1 \pm M)di_{L1}/dt$ and the equivalent inductance is $L_1 \pm M$. The direct coupling shows a large inductance $L_1 + M$ and the inverse coupling

Manuscript received August 5, 2010; revised October 10, 2010 and December 14, 2010; accepted January 5, 2011. Date of current version September 16, 2011. This work was supported by the LiteOn Technology Corporation, Nanjing, China. Recommended for publication by Associate Editor C. K. Tse.

F. Yang and Y. Yang are with the Aero-Power Sci-Tech Center, College of Automation Engineering, Nanjing University of Aeronautics and Astronautics, Nanjing 210016, China (e-mail: carryyangs@nuaa.edu.cn; zero3eddy@126.com).

X. Ruan is with the Aero-Power Sci-Tech Center, the College of Automation Engineering, Nanjing University of Aeronautics and Astronautics, Nanjing 210016, China, and also with the College of Electrical and Electronic Engineering, Huazhong University of Science and Technology, Wuhan 430074, China (e-mail: ruanxb@mail.hust.edu.cn).

Z. Ye is with LiteOn Technology Power SBG ATD-NJ R&D Center, Nanjing 210019, China (e-mail: sam.ye@liteon.com).

Digital Object Identifier 10.1109/TPEL.2011.2106165

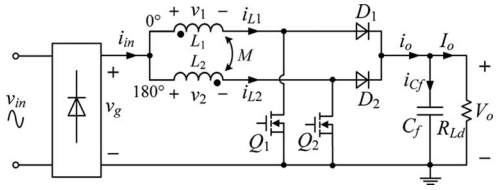

Fig. 2. Two-phase interleaved boost PFC converter with a coupled inductor.

shows a small inductance $L_1 - M$. In contrast, if $i_{L1} = -i_{L2}$, the direct coupling shows a small inductance $L_1 - M$ and the inverse coupling shows a large inductance $L_1 + M$. For this condition, if the two phases are operated at interleaved operation, the odd harmonics ($n = 1, 3, 5$, etc.) in i_{L1} and i_{L2} will be out of phase. Hence, inverse coupling leads to a larger equivalent inductance, which implies a reduction in the size of the coupled inductor.

B. Equivalent Inductances Derivation

Fig. 2 shows the interleaved CRM boost PFC converter with an inversely coupled inductor, where $v_{\rm in}$ is the input voltage, v_g is the rectified input voltage, and V_o is the output voltage.

It is assumed that the two windings of the coupled inductor are identical, i.e., $L_1 = L_2 = L_{\rm cp}$. The coupling coefficient is defined as $\alpha = M/L_{\rm cp}$. For inverse coupling, the sign before M in (1) is "$-$." From (1), we can obtain

$$v_1 + \alpha v_2 = (1-\alpha^2)L_{\rm cp}\frac{di_{L1}}{dt}. \tag{2}$$

At steady state, the conversion ratio for each switching cycle is

$$\frac{V_o}{v_g} = \frac{1}{1-d} \tag{3}$$

where d is the duty cycle of Q_1 and Q_2.

When Q_1 conducts, the voltage across winding 1, v_1 is v_g, and the current i_{L1} increases. di_{L1}/dt is positive and it is determined by the equivalent inductance. If Q_2 is OFF, the voltage across winding 2, v_2, is $v_g - V_o$; and if Q_2 conducts, $v_2 = v_g$.

Substituting $v_1 = v_g$, $v_2 = v_g - V_o$ and (3) into (2) yields

$$v_g = L_{\rm eq1}\frac{di_{L1}}{dt} \tag{4}$$

where

$$L_{\rm eq1} = \frac{1-\alpha^2}{1-\alpha d/(1-d)}L_{\rm cp}. \tag{5}$$

Substituting $v_1 = v_g$, $v_2 = v_g$ and (3) into (2) yields

$$v_g = L_{\rm eq2}\frac{di_{L1}}{dt} \tag{6}$$

where

$$L_{\rm eq2} = (1-\alpha)L_{\rm cp}. \tag{7}$$

So, when Q_1 conducts, the equivalent inductance is $L_{\rm eq1}$ and $L_{\rm eq2}$ when Q_2 is OFF and ON, respectively.

When Q_1 is OFF, the voltage across winding 1, v_1, is $v_g - V_o$, and the current i_{L1} decreases. The di_{L1}/dt is negative and it is determined by the equivalent inductance. Substituting $v_1 = v_g - V_o$, $v_2 = v_g - V_o$, and (3) into (2) yields

$$v_g - V_o = L_{\rm eq2}\frac{di_{L1}}{dt}. \tag{8}$$

Substituting $v_1 = v_g - V_o$ and $v_2 = v_g$, and (3) into (2) yields

$$v_g - V_o = L_{\rm eq3}\frac{di_{L1}}{dt} \tag{9}$$

where

$$L_{\rm eq3} = \frac{1-\alpha^2}{1-\alpha(1-d)/d}L_{\rm cp}. \tag{10}$$

Therefore, when Q_1 is OFF, the equivalent inductance is $L_{\rm eq2}$ and $L_{\rm eq3}$ when Q_2 is OFF and ON, respectively.

Similarly, the equivalent inductance for winding 2 can be derived. That is, when Q_2 conducts, the equivalent inductance is $L_{\rm eq1}$ and $L_{\rm eq2}$ when Q_1 is OFF and ON, respectively; and when Q_2 is OFF, the equivalent inductance is $L_{\rm eq2}$ and $L_{\rm eq3}$ when Q_1 is OFF and ON, respectively.

C. Inductor Current

Based on the equivalent inductance expressions and the voltages applied on the windings, the key waveforms of the interleaved CRM boost PFC converter with a coupled inductor are shown in Fig. 3. It is apparent that $L_{\rm eq1}$ and $L_{\rm eq3}$, respectively, determine the peak value of the inductor current when $d < 0.5$ and $d > 0.5$. According to (5) and (10), the relation between $L_{\rm eq1}$, $L_{\rm eq3}$, and d is shown in Fig. 4, in which $L_{\rm eq1}$ increases with d and $L_{\rm eq3}$ decreases with d, and $L_{\rm eq1}$ and $L_{\rm eq3}$ both reach the highest value at $d = 0.5$. It can be concluded that the coupling effects enlarge the equivalent inductance when the duty cycle come close to 0.5, thus leading to a smaller current ripple for a fixed switching frequency in CCM [15], [16] or a lower switching frequency for a fixed current ripple in CRM discussed as follows.

As shown in Fig. 3(a), the current decay slope are the same during $[t_1, t_2]$ and $[t_3, t_s]$, and the time intervals of $[t_1, t_2]$ and $[t_3, t_s]$ are the same, so the area between the current waveform and the time axis is equal to the shaded area. Hence, same as the noncoupled case, the peak current of each winding of the coupled inductor is twice its average value. Define $P_{\rm in}$ as the total input power of the two phases, and the input power of each phase is $P_{\rm in}/2$. So, the peak current of each winding of the coupled inductor can be expressed as

$$i_{L\_\rm pk} = 2i_{L\_\rm avg} = 2\sqrt{2}\frac{P_{\rm in}/2}{V_{\rm in}}|\sin\omega t| = \sqrt{2}\frac{P_{\rm in}}{V_{\rm in}}|\sin\omega t| \tag{11}$$

where $i_{L\_\rm pk}$ and $i_{L\_\rm avg}$ are the peak value and average value of the inductor current, respectively, $V_{\rm in}$ is the rms input voltage, $\omega = 2\pi f_{\rm line}$, and $f_{\rm line}$ is the frequency of the input voltage.

Since the amplitude of the inductor current is determined by the input power and the input voltage, it remains the same whether the inductors are coupled or not.

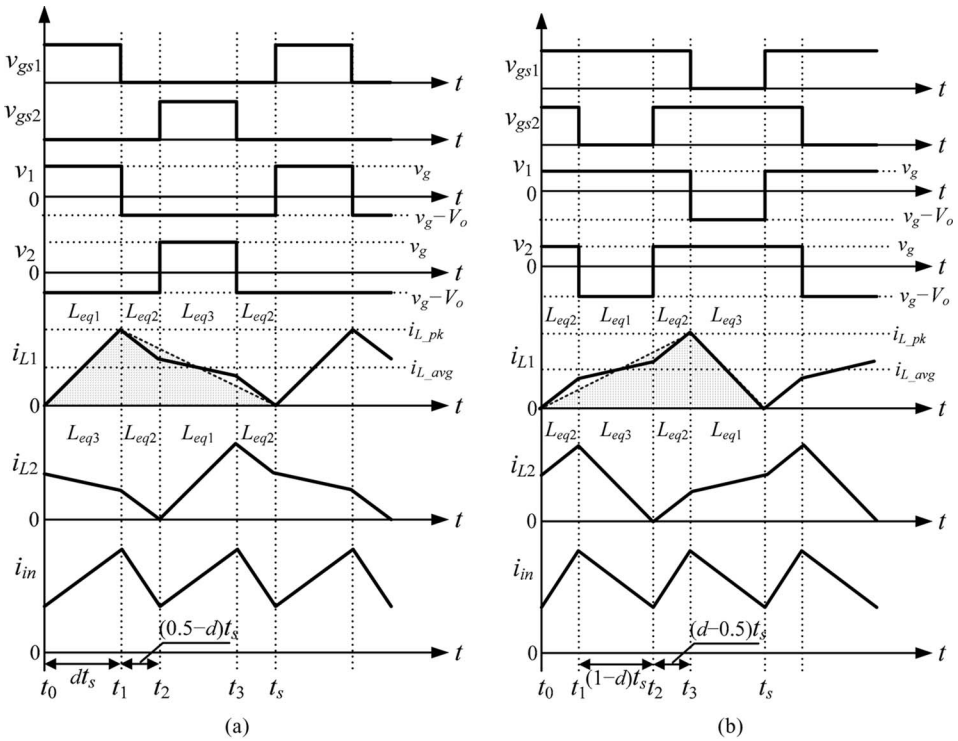

Fig. 3. Key waveforms of the interleaved CRM boost PFC converter with an inversely coupled inductor in (a) $d < 0.5$ and (b) $d > 0.5$.

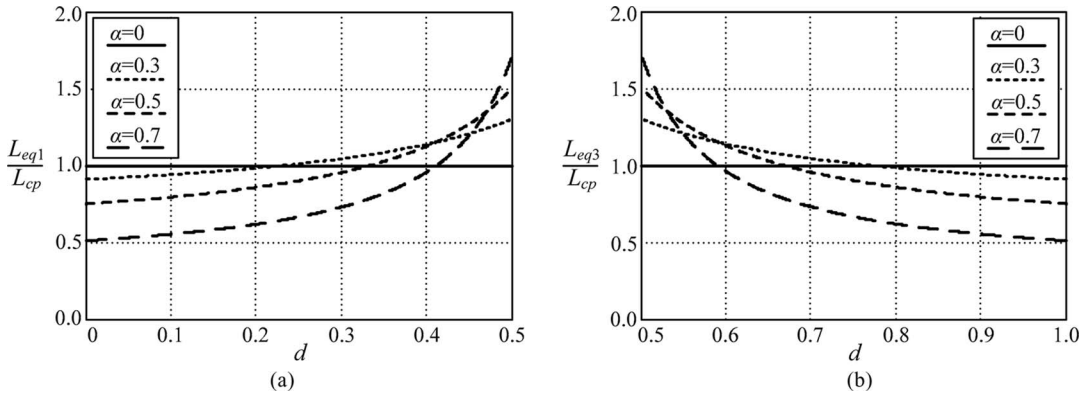

Fig. 4. Equivalent inductances vary with the duty cycle in (a) $d < 0.5$ and (b) $d > 0.5$.

D. Switching Frequency

For $d < 0.5$, the switch on-time can be derived from (4), i.e,

$$t_{\rm on} = \frac{L_{\rm eq1} i_{L\_\rm pk}}{v_g}. \tag{12}$$

Substitution of (11) and $v_g = \sqrt{2} V_{\rm in} |\sin \omega t|$ into (13) yields

$$t_{\rm on} = \frac{P_{\rm in} L_{\rm eq1}}{V_{\rm in}^2}. \tag{13}$$

Hence, the switching frequency is

$$f_s = \frac{1}{t_s} = \frac{1}{t_{\rm on}/d} = \frac{d V_{\rm in}^2}{P_{\rm in} L_{\rm eq1}}. \tag{14}$$

For $d > 0.5$, switch the off-time can be derived from (9), i.e,

$$t_{\rm off} = \frac{L_{\rm eq3} i_{L\_\rm pk}}{(V_o - v_g)}. \tag{15}$$

According to (3), we have $V_o = v_g/(1-d)$. Substitution of (11), $V_o = v_g/(1-d)$ and $v_g = \sqrt{2} V_{\rm in} |\sin \omega t|$ into (15) yields

$$t_{\rm off} = \frac{1-d}{d} \frac{P_{\rm in} L_{\rm eq3}}{V_{\rm in}^2}. \tag{16}$$

Hence, the switching frequency is

$$f_s = \frac{1}{t_s} = \frac{1}{t_{\rm off}/(1-d)} = \frac{d V_{\rm in}^2}{P_{\rm in} L_{\rm eq3}}. \tag{17}$$

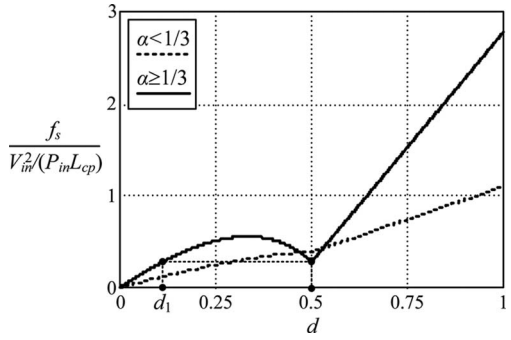

Fig. 5. Switching frequency varies with the duty cycle in different coupling coefficients ranges.

Substituting (5) and (10) into (14) and (17), respectively, the switching frequency can be expressed as

$$f_s = \begin{cases} \dfrac{V_{\rm in}^2}{P_{\rm in}L_{\rm cp}}\left[\dfrac{-(\alpha+1)d^2+d}{(1-\alpha^2)(1-d)}\right] & (d \le 0.5) \quad (18a) \\ \dfrac{V_{\rm in}^2}{P_{\rm in}L_{\rm cp}}\left[\dfrac{(1+\alpha)d-\alpha}{(1-\alpha^2)}\right] & (d > 0.5) \quad (18b) \end{cases}$$

that depends on $V_{\rm in}$, $P_{\rm in}$, $L_{\rm cp}$, d, and α. Since $L_{\rm cp}$ and α are fixed, for a given input power and input voltage, when the coupled inductor is well designed, the switching frequency varies with d in a half line period.

III. Coupling Effects on the Converter

A. Minimum Switching Frequency

Since the switching frequency of the CRM boost PFC converter with a coupled inductor is variable, in order to avoid audible noise, the minimum switching frequency $f_{s\_\min}$ should be higher than 20 kHz. Presuming that the self-inductance $L_{\rm cp}$ is fixed, the first term of (18), $V_{\rm in}^2/P_{\rm in}L_{\rm cp}$, is a constant for given $P_{\rm in}$ and $V_{\rm in}$. Hence, the switching frequency is determined by the second term of (18) that varies with d and α. As seen in (18b), when $d > 0.5$, f_s increases as d increases.

When $d \le 0.5$, in order to find the variation rule of f_s, it is necessary to know whether there is any turning point in the curve of f_s. Differentiating (18a) with d yields

$$\frac{\partial(f_s)}{\partial(d)} = \frac{V_{\rm in}^2}{P_{\rm in}L_{\rm cp}(1-\alpha^2)}\left[(1+\alpha) - \frac{\alpha}{(1-d)^2}\right]. \quad (19)$$

Setting (19) equals to zero, the turning point duty cycle can be calculated as

$$d = 1 - \sqrt{\frac{\alpha}{1+\alpha}}. \quad (20)$$

Substituting $d \le 0.5$ into (20) leads to $\alpha \ge 1/3$. That is to say, if $\alpha \ge 1/3$, there is a turning point in the curve of f_s. If $\alpha < 1/3$, substituting it and $d \le 0.5$ into (19) yields $\partial(f_s)/\partial(d) > 0$, which means f_s increases as d increases.

Fig. 5 shows the curves of the switching frequency versus duty cycle at different coupling coefficient ranges. It can be seen that if $\alpha < 1/3$, f_s increases as d increases over the whole range of d; if $\alpha \ge 1/3$, there is a turning point in the curve of f_s when $d \le 0.5$, and when $d > 0.5$, f_s increases as d increases.

According to (3), the duty cycle in a half line cycle can be expressed as

$$d = 1 - \sqrt{2}V_{\rm in}\frac{|\sin\omega t|}{V_o}. \quad (21)$$

At the peak of the rectified input voltage, $|\sin\omega t| = 1$, the duty cycle get its minimum value, i.e.,

$$d_{\min} = 1 - \frac{\sqrt{2}V_{\rm in}}{V_o} \quad (22)$$

and at the zero cross of the input voltage, $|\sin\omega t| = 0$, the duty cycle get its maximum value of 1. That is to say, the duty cycle ranges from $d_{\min}$ to 1 in a half line cycle.

According to (22), if $V_{\rm in} < V_o/(2\sqrt{2})$, $d_{\min} > 0.5$. As seen in Fig. 5, when $d > 0.5$, the switching frequency increases with d, and the minimum switching frequency $f_{s\_\min}$ occurs at the minimum duty cycle, $d_{\min}$. Substitution of (22) into (18b), $f_{s\_\min}$ is derived as

$$f_{s\_\min}|_{d_{\min}} = \frac{V_{\rm in}^2}{P_{\rm in}L_{\rm cp}}\frac{V_o - \sqrt{2}V_{\rm in}(1+\alpha)}{(1-\alpha^2)V_o}. \quad (23)$$

If $V_{\rm in} \ge V_o/\left(2\sqrt{2}\right)$, $d_{\min} \le 0.5$. As seen in Fig. 5, $f_{s\_\min}$ would occur at two possible duty cycles: one is 0.5, and the other is $d_{\min}$. The boundary value is d_1, of which the switching frequency is equal to that of $d = 0.5$, and it can be derived by $f_s(d = d_1) = f_s(d = 0.5)$ using (18a) as

$$d_1 = \frac{1-\alpha}{1+\alpha}. \quad (24)$$

If $d_1 \le d_{\min} \le 0.5$, $f_{s\_\min}$ occurring at $d = 0.5$ can be calculated as

$$f_{s\_\min}|_{d=0.5} = V_{\rm in}^2 P_{\rm in}L_{\rm cp}\frac{1}{2(1+\alpha)}. \quad (25)$$

If $d_{\min} < d_1 < 0.5$, $f_{s\_\min}$ occurring at $d = d_{\min}$ can be calculated by substituting (22) into (18a) as

$$f_{s\_\min}|_{d_{\min}} = \frac{V_{\rm in}}{P_{\rm in}L_{\rm cp}}\frac{-\alpha\left(V_o - \sqrt{2}V_{\rm in}\right)^2 + \sqrt{2}V_{\rm in}V_o - 2V_{\rm in}^2}{(1-\alpha^2)\sqrt{2}V_o}. \quad (26)$$

From (22) and (24), when $d_{\min} \ge d_1$, the input voltage meets

$$V_{\rm in} \le \frac{\sqrt{2}V_o\alpha}{\alpha+1}. \quad (27)$$

Based on the aforementioned analysis, the following conclusions can be drawn.

1) When $\alpha \in [0, 1/3]$: if $V_{\rm in} < V_o/(2\sqrt{2})$, $f_{s\_\min}$ is calculated by (23); if $V_{\rm in} \ge V_o/(2\sqrt{2})$, $f_{s\_\min}$ is calculated by (26).
2) When $\alpha \in [1/3, 1]$: if $V_{\rm in} < V_o/(2\sqrt{2})$, $f_{s\_\min}$ is calculated by (23); if $V_o/\left(2\sqrt{2}\right) \le V_{\rm in} \le \sqrt{2}V_o\alpha/(\alpha+1)$, $f_{s\_\min}$ is calculated by (25); if $V_{\rm in} > \sqrt{2}V_o\alpha/(\alpha+1)$, $f_{s\_\min}$ is calculated by (26).

Fig. 6 depicts $f_{s\_\min}$ over the whole input voltage range for different coupling coefficients when $V_o = 400$ V. As seen, the values at $V_{\rm in} = V_{\rm in\_min}$, $V_{\rm in} = V_o/\left(2\sqrt{2}\right)$ and $V_{\rm in} = V_{\rm in\_max}$

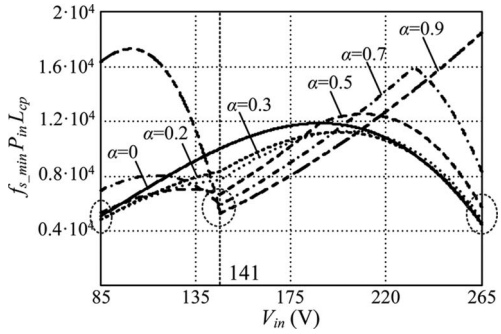

Fig. 6. Minimum switching frequency varies with the input voltages in different coupling coefficients.

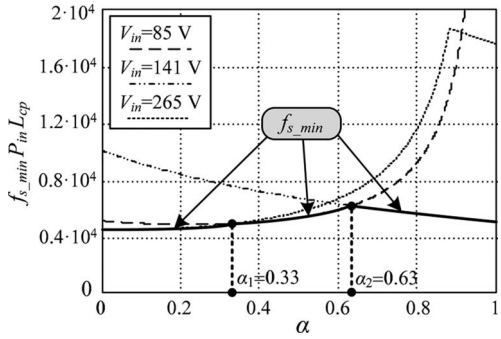

Fig. 7. Minimum switching frequency varies with coupling coefficients.

are relatively lower than those of other cases. $f_{s\_\min}$ varying with the coupling coefficient at the aforementioned three input voltages are plotted in Fig. 7, and the lowest value among them is chosen to be the minimum switching frequency corresponding to the specific coupling coefficient as shown by the solid line in Fig. 7. If $L_{\rm cp}$ is fixed, the minimum frequency of the coupled case is always higher than that of the noncoupled case. Therefore, coupling does not lead to any audio noise.

The minimum switching frequency in this paper can be expressed as shown (28), at the bottom of this page, where α_1 and α_2 are the corresponding coupling coefficients of the cross points between the curves of $V_{\rm in\_min}$ and $V_{\rm in\_max}$ and between the curves of $V_{\rm in\_min}$ and $V_o/(2\sqrt{2})$. They can be calculated as

$$\alpha_1 = \frac{\sqrt{2}V_o V_{\rm in\_max}^2 + 2V_{\rm in\_min}^3 - 2V_{\rm in\_max}^3 - \sqrt{2}V_o V_{\rm in\_min}^2}{2V_o V_{\rm in\_max}^2 - V_o^2 V_{\rm in\_max} + 2V_{\rm in\_min}^3 - 2V_{\rm in\_max}^3} \tag{29}$$

$$\alpha_2 = \frac{V_o^3 + 16\sqrt{2}V_{\rm in\_min}^3 - 16V_{\rm in\_min}^2 V_o}{V_o^3 - 16\sqrt{2}V_{\rm in\_min}^3}. \tag{30}$$

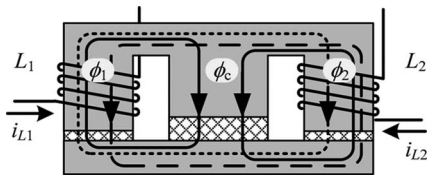

Fig. 8. Windings and the core structure of the coupled inductor.

For $V_{\rm in\_min} = 85\ V_{\rm rms}$, $V_{\rm in\_max} = 265\ V_{\rm rms}$, and $V_o = 400$ V, $\alpha_1 = 0.33$ and $\alpha_2 = 0.63$.

B. Flux Linkage and the Turns Number

The windings and core structure of the coupled inductor are shown in Fig. 8. The winding structure is symmetric, i.e., $L_1 = L_2 = L_{\rm cp}$, the turns number is $N_1 = N_2 = N_{\rm cp}$, the outer leg air gap is $\delta_1 = \delta_2 = \delta_s$, and the center leg air gap is δ_c. The coupling coefficient can be achieved by adjusting the air gap ratio. The noncoupled inductor is a special case for this structure featuring $\delta_c = 0$. For the same magnetic core, the maximum flux is fixed. Therefore, the turns number is proportional to the flux linkage of the corresponding leg.

According to Fig. 8, the flux linkages of the outer legs and the center leg can be described as [11]

$$\begin{cases} \psi_1 = \phi_1 N_{\rm cp} = L_{\rm cp} i_{L1} - \alpha L_{\rm cp} i_{L2} \\ \psi_2 = \phi_2 N_{\rm cp} = L_{\rm cp} i_{L2} - \alpha L_{\rm cp} i_{L1} \\ \psi_c = \psi_1 + \psi_2 = (1-\alpha) L_{\rm cp}(i_{L1} + i_{L2}) \end{cases} \tag{31}$$

and they are plotted in Fig. 9, for $d < 0.5$ as an example, based on the inductor current waveforms in Fig. 3(a).

Since the two inductor current values at t_1 can be calculated from (8), (11), and (18), the peak flux linkage Ψ_s of the outer leg is

$$\psi_s = \begin{cases} \dfrac{L_{\rm cp} P_{\rm in} V_o}{2V_{\rm in}^2}\left[(1-d)(1-\alpha)\left(2 + \dfrac{\alpha}{1-(1+\alpha)d}\right)\right] & (d \le 0.5) \quad (32a) \\ \dfrac{L_{\rm cp} P_{\rm in} V_o}{2V_{\rm in}^2}\left[(1-d)(1-\alpha)\left(2 + \dfrac{\alpha}{(1+\alpha)d-\alpha}\right)\right] & (d > 0.5) \quad (32b) \end{cases}$$

$$f_{s\_\min} = \begin{cases} \dfrac{V_{\rm in\_max}\left[-\alpha\left(V_o - \sqrt{2}V_{\rm in\_max}\right)^2 + \sqrt{2}V_{\rm in\_max}V_o - 2V_{\rm in\_max}^2\right]}{P_{\rm in} L_{\rm cp}(1-\alpha^2)\sqrt{2}V_o} & (0 \le \alpha \le \alpha_1) \\ \dfrac{V_{\rm in\_min}^2\left[V_o - \sqrt{2}V_{\rm in\_min}(1+\alpha)\right]}{P_{\rm in} L_{\rm cp}(1-\alpha^2)V_o} & (\alpha_1 < \alpha \le \alpha_2) \\ \dfrac{V_o^2}{16 P_{\rm in} L_{\rm cp}(1+\alpha)} & (\alpha_2 \le \alpha \le 1) \end{cases} \tag{28}$$

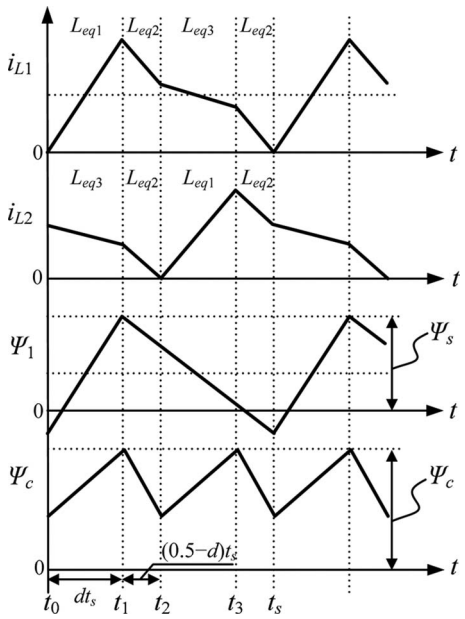

Fig. 9. Flux linkage waveforms of the outer legs and center leg.

and the peak flux linkage Ψ_c in the center leg is

$$\psi_c = \begin{cases} \dfrac{L_{\rm cp}P_{\rm in}V_o}{2V_{\rm in}^2}(1-d)(1-\alpha)\left(\dfrac{4+\alpha-1}{1-(1+\alpha)d}\right) \\ \qquad\qquad (d \le 0.5) \\ \dfrac{L_{\rm cp}P_{\rm in}V_o}{2V_{\rm in}^2}(1-d)(1-\alpha)\left(4+\dfrac{\alpha-1}{(1+\alpha)d-\alpha}\right) \\ \qquad\qquad (d \le 0.5) \end{cases} \tag{33}$$

The flux densities of the outer leg and the center leg are, respectively, $B_s = \Psi_s/(N_{\rm cp}\ A_e)$ and $B_c = \Psi_c/(N_{\rm cp}\cdot 2A_e)$, where A_e is the effective cross section of the outer leg. The ratio of the flux densities can be expressed as

$$\frac{B_s}{B_c} = \begin{cases} 1-\dfrac{1+\alpha}{4(1+\alpha)d-3-\alpha} & (d \le 0.5) \quad (34a) \\ 1+\dfrac{1+\alpha}{4(1+\alpha)d-1-3\alpha} & (d > 0.5) \quad (34b) \end{cases}$$

If $4(1+\alpha)d-3-\alpha=0$ in (34a), $d=0.5+(1-\alpha)/(4+4\alpha)$ which is no less than 0.5. For $d \le 0.5$, $4(1+\alpha)d-3-\alpha \le 0$ and (34a) is larger than 1, which means the flux density of the outer leg is always higher than that of the center leg. The same conclusion can be drawn for $d > 0.5$. So, the worst case of the core occurs at the outer leg and the turns number design should base on the maximum flux linkage $\Psi_{\max}$ of the outer leg.

If the self-inductance is fixed, i.e., the first term of (32), $[L_{\rm cp}P_{\rm in}V_o/(2V_{\rm in}^2)]$, is constant for a given $P_{\rm in}$, $V_{\rm in}$, and V_o. Hence, the flux linkage is dependent on the second term of (32) that varies with d and α. In order to find the variation rule of

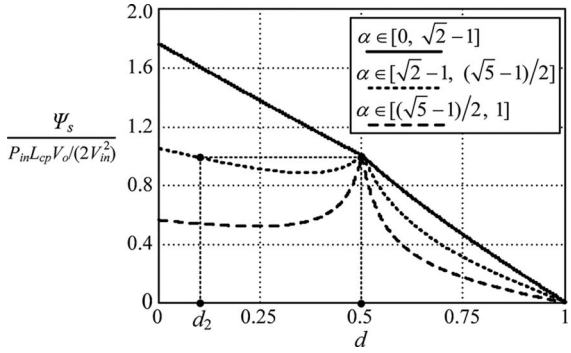

Fig. 10. Flux linkage of the outer leg varies with the duty cycle in different coupling coefficients.

Ψ_s, the deferential of (32) over d is derived as

$$\frac{\partial(\psi_s)}{\partial(d)} = \begin{cases} \dfrac{L_{\rm cp}P_{\rm in}V_o(1-\alpha)}{2V_{\rm in}^2}\left(\dfrac{-2+\alpha^2}{(-(1+\alpha)d+1)^2}\right) \\ \qquad\qquad (d \le 0.5) \quad (35a) \\ \dfrac{L_{\rm cp}P_{\rm in}V_o(1-\alpha)}{2V_{\rm in}^2}\left(-2-\dfrac{\alpha}{((1+\alpha)d-\alpha)^2}\right) \\ \qquad\qquad (d > 0.5) \quad (35b) \end{cases}$$

As seen in (35b), when $d > 0.5$, $\partial(\Psi_s)/\partial(d) < 0$, and Ψ_s decreases as d increases.

Setting (35a) equals to zero, the turning point duty cycle can be obtained as

$$d = \frac{\sqrt{2}-\alpha}{\sqrt{2}(1+\alpha)}. \tag{36}$$

Substituting $d \le 0.5$ into (36) leads to $\alpha \ge \sqrt{2}-1$. That is to say, if $\alpha \ge \sqrt{2}-1$, there is a turning point in the curve of Ψ_s. If $\alpha < \sqrt{2}-1$, substituting it and $d \le 0.5$ into (35a) yields $\partial(\Psi_s)/\partial(d) < 0$, which means Ψ_s decreases as d increases.

When $\alpha \ge \sqrt{2}-1$, there is a turning point in the curve of Ψ_s, which means $\Psi_{\max}$ would occur at two possible duty cycles: one is 0.5, and the other is $d_{\min}$. Define the boundary value d_2, of which Ψ_s is equal to that of $d=0.5$, and it can be derived by $\Psi_s(d=d_2)=\Psi_s(d=0.5)$ using (32a) as

$$d_2 = \frac{\alpha^2+\alpha-1}{\alpha^2-1}. \tag{37}$$

Substituting $0 \le d_2 \le 0.5$ into (37) leads to $\alpha \le (\sqrt{5}-1)/2$. That is to say, if $\sqrt{2}-1 \le \alpha \le (\sqrt{5}-1)/2$, there is a d_2 which makes $\Psi_s(d=d_2)=\Psi_s(d=0.5)$. If $(\sqrt{5}-1)/2 < \alpha \le 1$, substituting it and $d \le 0.5$ into (32), it can be found that $\Psi_s(d) < \Psi_s(d=0.5)$ over the whole range of d.

Fig. 10 shows the curves of the flux linkage versus duty cycle at different coupling coefficient ranges. It can be seen that if $\alpha < \sqrt{2}-1$, Ψ_s increases as d increases over the whole range of d; if $\sqrt{2}-1 \le \alpha \le \left(\sqrt{5}-1\right)/2$, when $d \le 0.5$, there is a turning point in the curve of Ψ_s, and when $d > 0.5$, Ψ_s decreases as d increases; if $\left(\sqrt{5}-1\right)/2 < \alpha \le 1$, $\Psi_s(d) \le \Psi_s(d=0.5)$.

According to (22), when $V_{\rm in} < V_o/\left(2\sqrt{2}\right)$, $d_{\min} > 0.5$. Ψ_s increases as d increases and the maximum flux linkage $\Psi_{\max}$

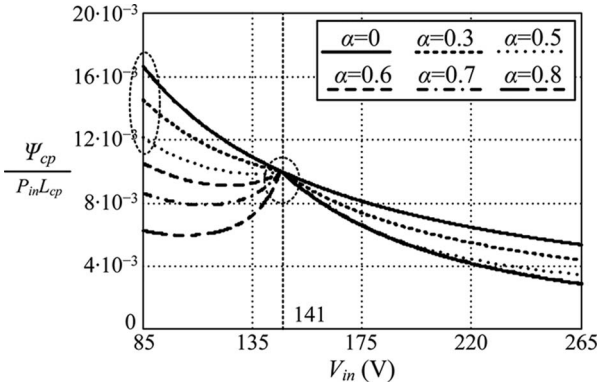

Fig. 11. Flux linkage varies with input voltage in different coupling coefficients.

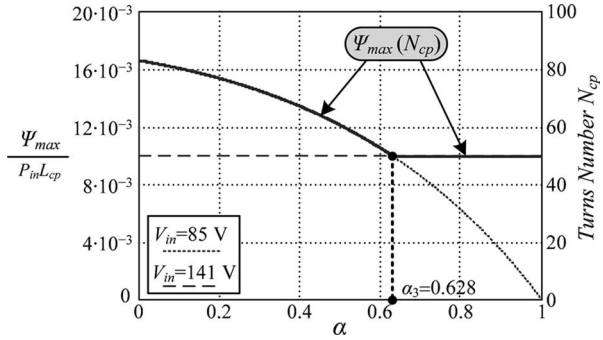

Fig. 12. Maximum flux linkage and the turns' number vary with different coupling coefficients.

occurs at $d = d_{\min}$. Substitution (22) into (32b), $\Psi_{\max}$ can be calculated by as

$$\psi_{\max}|_{d_{\min}} = \frac{P_{\text{in}} L_{\text{cp}}}{\sqrt{2} V_{\text{in}}} \left[(1-\alpha) + \frac{1-\alpha^2}{1-\alpha\sqrt{2}V_{\text{in}}/\left(V_o - \sqrt{2}V_{\text{in}}\right)} \right]. \quad (38)$$

When $V_{\text{in}} \geq V_o/(2\sqrt{2})$, $d_{\min} \leq 0.5$. If $d_2 \leq d_{\min} \leq 0.5$, $\Psi_{\max}$ occurs at $d = 0.5$, and it can be calculated as

$$\psi_{\max}|_{d=0.5} = \frac{P_{\text{in}} L_{\text{cp}} V_o}{2V_{\text{in}}^2}. \quad (39)$$

If $d_{\min} < d_2 < 0.5$, $\Psi_{\max}$ occurs at $d = d_{\min}$, and it can be calculated by substitution of (22) into (32a) as

$$\psi_{\max}|_{d_{\min}} = \frac{P_{\text{in}} L_{\text{cp}}}{\sqrt{2} V_{\text{in}}} \left[(1-\alpha) + \frac{1-\alpha^2}{1-\alpha\left(V_o - \sqrt{2}V_{\text{in}}\right)/\left(\sqrt{2}V_{\text{in}}\right)} \right]. \quad (40)$$

From (20) and (35), when $d_{\min} \geq d_2$, the input voltage meets

$$V_{\text{in}} \leq \frac{V_o \alpha}{\sqrt{2}(1-\alpha^2)}. \quad (41)$$

Based on the aforementioned analysis, the following conclusions can be drawn.

1) When $\alpha \in [0, \sqrt{2}-1]$: if $V_{\text{in}} < V_o/(2\sqrt{2})$, $\Psi_{\max}$ is calculated by (38); if $V_{\text{in}} \geq V_o/(2\sqrt{2})$, $\Psi_{\max}$ is calculated by (40).
2) When $\alpha \in [\sqrt{2}-1, (\sqrt{5}-1)/2]$: if $V_{\text{in}} < V_o/(2\sqrt{2})$, $\Psi_{\max}$ is calculated by (38); if $V_o/(2\sqrt{2}) \leq V_{\text{in}} \leq V_o\alpha/[\sqrt{2}(1-\alpha^2)]$, $\Psi_{\max}$ is calculated by (39); if $V_{\text{in}} > V_o\alpha/[\sqrt{2}(1-\alpha^2)]$, $\Psi_{\max}$ is calculated by (40).
3) When $\alpha \in [(\sqrt{5}-1)/2, 1]$, $\Psi_{\max}$ is calculated by (39) over the whole input voltage range.

$\Psi_{\max}$ varying with the input voltage for different coupling coefficients can be calculated and is shown in Fig. 11. It is shown that over the whole input voltage range, the $\Psi_{\max}$ at $V_{\text{in}} = V_o/(2\sqrt{2})$ or $V_{\text{in}} = V_{\text{in\_min}}$ of any specific coupling coefficient are relatively higher than those of other cases. The $\Psi_{\max}$ varying with the coupling coefficient at the two aforementioned voltages are plotted in Fig. 12, and the higher value between them is chosen to be the maximum $\Psi_{\max}$ point as the solid line shows. Since the flux linkage is reduced in a specific coupling coefficient range and the same core is used in both coupled and noncoupled cases, the turns number $N_{\text{cp}} = \Psi_{\max}/\phi$ can be reduced by coupling as shown in Fig. 12.

The maximum flux linkage can be expressed as

$$\psi_{\max} = \begin{cases} \dfrac{P_{\text{in}} L_{\text{cp}}(1-\alpha)}{\sqrt{2}V_{\text{in\_min}}} \dfrac{(2+\alpha)V_o - 2(1+\alpha)\sqrt{2}V_{\text{in\_min}}}{V_o - \sqrt{2}V_{\text{in\_min}} - \alpha\sqrt{2}V_{\text{in\_min}}} & (0 \leq \alpha \leq \alpha_3) \\ \dfrac{4P_{\text{in}} L_{\text{cp}}}{V_o} & (\alpha_3 < \alpha \leq 1) \end{cases} \quad (42)$$

where α_3 is the corresponding coefficient of the cross point between the curves of $V_{\text{in\_min}}$ and $V_o/(2\sqrt{2})$, and it can be calculated by (43) as shown, at the bottom of this page, when $V_{\text{in\_min}} = 85$ V and $V_o = 400$ V, $\alpha_3 = 0.628$.

C. Input Current Ripple

The inductor current ripple of each phase, which is equal to the inductor current peak value, can be expressed as

$$\Delta i_{L\_\text{cp}} = \begin{cases} \dfrac{v_g}{L_{\text{eq1}}} dt_s & (d \leq 0.5) \\ \dfrac{V_o - v_g}{L_{\text{eq3}}}(1-d)t_s & (d > 0.5). \end{cases} \quad (44)$$

$$\alpha_3 = \frac{\sqrt{64V_{\text{in\_min}}^4 - 64\sqrt{2}V_{\text{in\_min}}^3 V_o + 112V_{\text{in\_min}}^2 V_o^2 - 40\sqrt{2}V_{\text{in\_min}}V_o^3 - 9V_o^4}}{2V_o^2 - 4\sqrt{2}V_o V_{\text{in\_min}}} + \frac{8\sqrt{2}V_o V_{\text{in\_min}}^2 - V_o^2}{2V_o^2 - 4\sqrt{2}V_o V_{\text{in\_min}}} \quad (43)$$

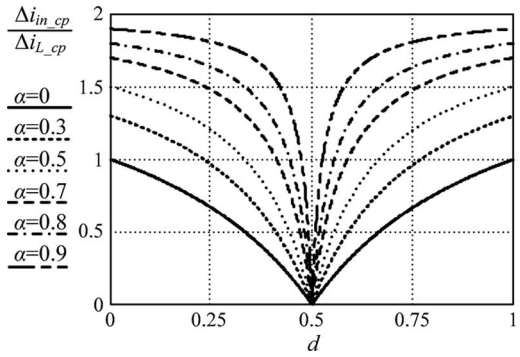

Fig. 13. Ratio of the input ripple current and the inductor ripple current in different coupling coefficients.

The input current is the sum of the two inductor currents. As shown in Fig. 3, the input current ripple can be described as

$$\Delta i_{\text{in\_cp}} = \begin{cases} 2\dfrac{(V_o - v_g)}{L_{\text{eq2}}}(0.5-d)t_s & (d \le 0.5) \\ 2\dfrac{v_g}{L_{\text{eq}^2}}(d-0.5)t_s & (d > 0.5). \end{cases} \tag{45}$$

From (45), L_{eq2}, relating to α and L_{cp}, determines the input current ripple. The ratio of the input current ripple and the inductor current ripple can be obtained from (44) and (45) as

$$\frac{\Delta i_{\text{in\_cp}}}{\Delta i_{L\_\text{cp}}} = \begin{cases} \dfrac{(1-2d)(1+\alpha)}{(1-d)-\alpha d} & (d \le 0.5) \\ \dfrac{(2d-1)(1+\alpha)}{d-\alpha(1-d)} & (d > 0.5) \end{cases} \tag{46}$$

and it is plotted in Fig. 13 for different coupling coefficients. As seen, the input current ripple increases when the inductors are coupled, and the stronger the coupling is, the higher the input currents ripple will be. This may lead to a larger differential-mode (DM) EMI filter, which is a disadvantage for the coupled inductor.

D. Reasonable Coupling Coefficient Selection

The proper selection of coupling coefficient is based on the coupling effects on the converter. The turns number can be reduced by coupling as shown in Fig. 12. So a relatively strong coupling is desired. In contrast, since the input current ripple is increased as shown in Fig. 13 and the switching frequency is changed by coupling, a larger DM EMI filter may be needed. Therefore, a compromising coupling coefficient is desired to balance simultaneously the volume and cost of both the EMI filter and the coupled inductor. Furthermore, in terms of the fabrication of EE or EI core, the one featuring three legs with the same air gap, which means $\alpha = 1/3$, is preferred. Hence, we choose $\alpha = 1/3$ in this paper.

L_{cp} and M are expressed as [11]

$$\begin{cases} L_{\text{cp}} = \dfrac{N_{\text{cp}}^2(R_s+R_c)}{R_s(R_s+2R_c)} = \dfrac{N_{\text{cp}}^2}{R_s(1+\alpha)} & \text{(47a)} \\ M = \dfrac{N_{\text{cp}}^2 R_c}{R_s(R_s+2R_c)} & \text{(47b)} \end{cases}$$

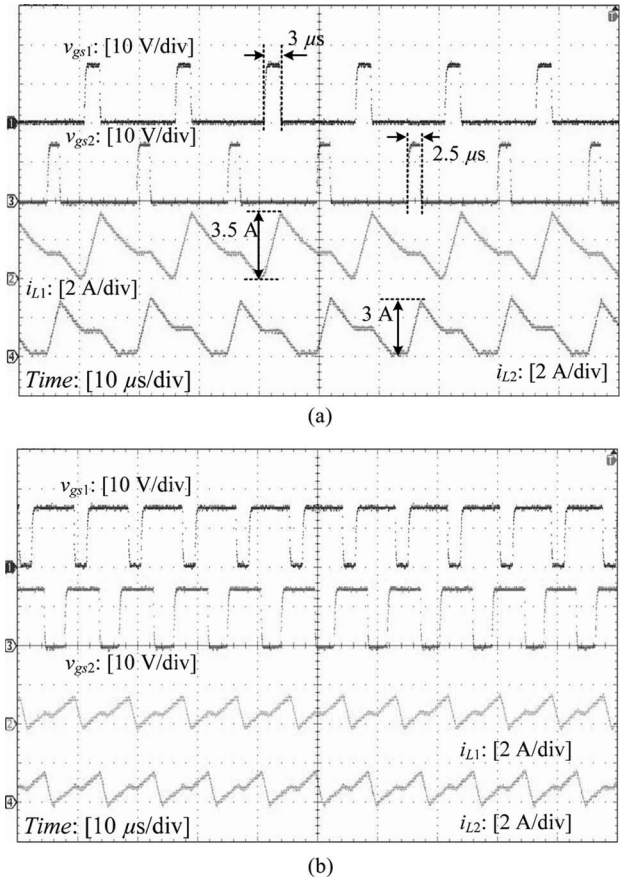

Fig. 14. Experimental waveforms of the coupled inductor currents in (a) $d < 0.5$ and (b) $d > 0.5$.

where the outer leg reluctance $R_s = \delta_s/(\mu_0 A_e)$ and the center leg reluctance $R_c = \delta_c/(\mu_0 \cdot 2A_e)$.

Substituting R_s into (47a), the air gap of the outer leg is

$$\delta_s = \frac{N_{\text{cp}}^2 \mu_0 A_e}{L_{\text{cp}}(1+\alpha)}. \tag{48}$$

Since $\alpha = M/L_{\text{cp}} = R_c/(R_s + R_c)$, the air gap of the center leg is

$$\delta_c = 2\delta_s \frac{\alpha}{1-\alpha}. \tag{49}$$

IV. Experimental Verification

Since the equivalent inductance of the coupled inductor varies in a half line period, in order to achieve unity PF, the switch on-time should not be constant. Therefore, the current-mode control [8], which makes the peak value of the inductor current be sinusoidal is more reasonable than the voltage-mode control, which only fixes the switch on-time. A 300-W two-phase interleaved CRM boost PFC converter is constructed to verify the aforementioned analysis. The output voltage is set at 400 V, the minimum frequency is 45 kHz, and the control IC is CHAMPION CM6565 which functions in a similar way of two L6561 with 180° phase shift of their output signals. The coupled inductor is fabricated by one EI40/35 ferrite core $L_{\text{cp}} = 330\ \mu$H, $\alpha = 1/3$, and $N_{\text{cp}} = 63$. The noncoupled inductor is fabricated by the same core $L_{\text{nc}} = 330\ \mu$H and $N_{\text{nc}} = 74$. Since the same wire is used in both cases, the coupled case has a lower copper

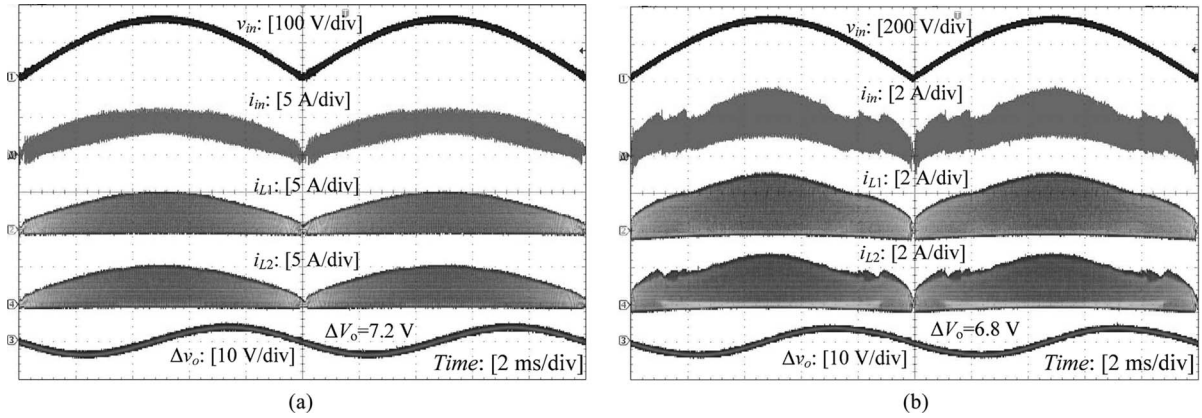

Fig. 15. Experimental waveforms of the input currents and inductor currents with discrete inductors in (a) $V_{\rm in} = 110$ V and (b) $V_{\rm in} = 220$ V.

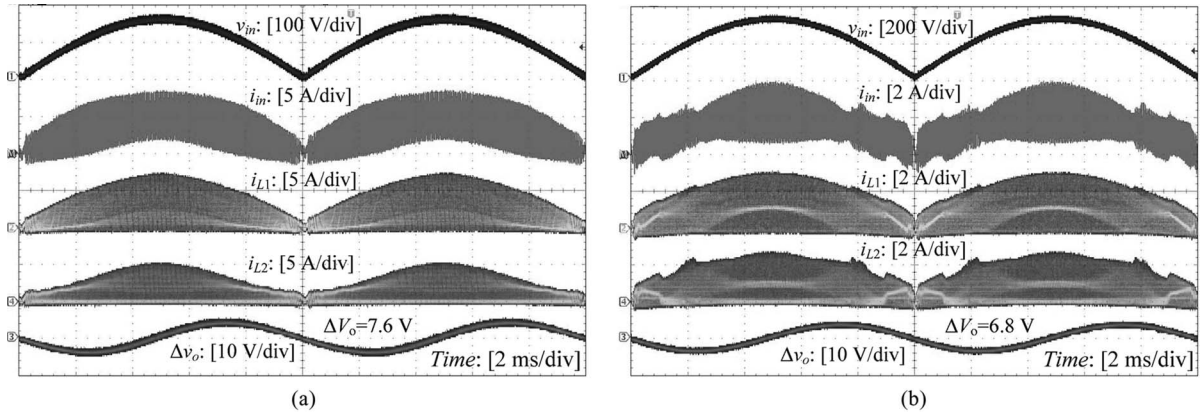

Fig. 16. Experimental waveforms of the input current and inductor currents with couple inductors in (a) $V_{\rm in} = 110$ V and (b) $V_{\rm in} = 220$ V.

consumption than the noncoupled case. In practical circuit, L_1 and L_2 can not be identical. The difference of the two inductors will leads to unbalanced power sharing between the two phases, so we tried to make the two inductors be as equal as possible.

Fig. 14 shows the inductor currents with different duty cycles. The control IC only keeps the master phase to operate in the current-mode and provides the drive signal of the slave phase by the internal phase shifting circuits directly. In the ideal case, the two-phase currents should be both in CRM. However, in order to prevent the inductor current i_{L2} from entering CCM, the control IC intentionally makes the on-time of the slave phase (corresponding to phase 2 here) be shorter than that of the master phase (which is phase 1 here), thus the peak value of i_{L2} is slightly smaller than that of i_{L1}, and i_{L2} reduces to zero before turning on Q_2. i.e., i_{L1} is exactly in CRM and i_{L2} is in DCM. Such phenomenon occurs easily at high line, where the duty cycle is small.

Figs. 15 and 16 show the inductor currents, the input currents and output voltage ripple in the noncoupled and coupled cases with different input voltages at full load. Since the $L_{\rm eq2}$ is reduced through the proposed design, the input current ripple in the coupled case is larger than that in the noncoupled case. Since the control IC strategy aforementioned, the peak value of the inductor current of the slave phase is lower than that of the master phase and the power sharing is unequal between the two phases as shown in Fig. 16(a). The output filter capacitor is used to balance the instantaneous input power and the constant output power, and the output voltage has a ripple with the frequency of twice the line frequency. The difference between the coupled-inductor and noncoupled inductors is the high switching frequency current ripple, and it has no effective effect on the output voltage ripple, which can be seen in Figs. 15 and 16.

V. Conclusion

In this paper, the coupled inductor is introduced to the two-phase interleaved CRM boost PFC converter, and some coupling effects are analyzed. Compared with the noncoupled inductor, if the self-inductance and the magnetic core are the same, the minimum switching frequency of the coupled inductor is still higher than 20 kHz, and the flux linkage is reduced, implying a reduction of the turns' number. Therefore, the cost of the inductors can be reduced by coupling. The control strategy of the interleaved CRM boost PFC converter with a coupled inductor should adopt the current-mode strategy since the equivalent inductance varies with time in a half line period and the switch on-time should be also time-variant for unity PF.

Since the input current ripple is increased and the switching frequency is changed by coupling, the DM EMI filter design should be further considered together with the coupled inductor

for minimizing the total volume and cost of the magnetic components. For a more comprehensive design, the high-frequency effects on the windings and the current waveform variations on the rms value should be considered.

REFERENCES

[1] J. S. Lai and D. Chen, "Design consideration for power factor correction boost converter operating at the boundary of continuous conduction mode and discontinuous conduction mode," in *Proc. IEEE Appl. Power Electron. Conf.*, 1993, pp. 267–273.

[2] B. A. Miwa, D. M. Otten, and M. F. Schlecht, "High efficiency power factor correction using interleaving techniques," in *Proc. IEEE Appl. Power Electron. Conf.*, 1992, pp. 557–568.

[3] L. Balogh and R. Redl, "Power-factor correction with interleaved boost converters in continuous-inductor-current mode," in *Proc. IEEE Appl. Power Electron. Conf.*, 1993, pp. 168–174.

[4] M. S. Elmore, "Input current rippled cancellation in synchronized, parallel connected critically continuous boost converters," in *Proc. IEEE Appl. Power Electron. Conf.*, 1996, pp. 152–158.

[5] T. Ishii and Y. Mizutani, "Power factor correction using interleaving technique for critical mode switching converters," in *Proc. IEEE Power Electron. Spec. Conf.*, 1998, pp. 905–910.

[6] P. A. Dahono, S. Riyadi, A. Mudawari, and Y. Haroen, "Output ripple analysis of multiphase dc–dc converter," in *Proc. IEEE Power Electron. Drive Syst. Conf.*, 1999, pp. 626–631.

[7] J. R. Tsai, T. F. Wu, C. Y. Wu, Y. M. Chen, and M. C. Lee, "Interleaving phase shifters for critical-mode boost PFC," *IEEE Trans. Power Electron.*, vol. 23, no. 3, pp. 1348–1357, May 2008.

[8] L. Huber, B. T. Irving, and M. M. Jovanović, "Open-loop control method for interleaved DCM/CCM boundary boost PFC converter," *IEEE Trans. Power Electron.*, vol. 23, no. 4, pp. 1649–1657, Jul. 2008.

[9] L. Huber, B. T. Irving, and M. M. Jovanović, "Review and stability analysis of PLL-based interleaving control of DCM/CCM boundary boost PFC converter," *IEEE Trans. Power Electron.*, vol. 24, no. 8, pp. 1992–1999, Aug. 2009.

[10] X. Xu, W. Liu, and A. Q. Huang, "Two-phase interleaved critical mode PFC boost converter with closed loop interleaving strategy," *IEEE Trans. Power Electron.*, vol. 24, no. 12, pp. 3003–3013, Dec. 2009.

[11] P. L. Wong, P. Xu, P. Yang, and F. C. Lee, "Performance improvements of interleaving VRMs with coupling inductors," *IEEE Trans. Power Electron.*, vol. 16, no. 4, pp. 499–507, Jul. 2001.

[12] J. Li, C. R. Sullivan, and A. Schultz, "Coupled inductor design optimization for fast-response low-voltage dc–dc converters," in *Proc. IEEE Appl. Power Electron. Conf.*, 2002, pp. 817–823.

[13] P. Zumel, O. Garcia, J. A. Cobos, and J. Uceda, "Magnetic integration for interleaved converters," in *Proc. IEEE Appl. Power Electron. Conf.*, 2003, pp. 1143–1149.

[14] J. W. Kolar, G. R. Kamath, N. Mohan, and F. C. Zach, "Self-adjusting input current ripple cancellation of coupled parallel connected hysteresis-controlled boost power factor correctors," in *Proc. IEEE Power Electron. Spec. Conf.*, 1998, pp. 164–173.

[15] S. Chandrasekaran and L. U. Gokdere, "Integrated magnetics for interleaved dc–dc boost converter for fuel cell powered vehicles," in *Proc. IEEE Power Electron. Spec. Conf.*, 2004, pp. 356–361.

[16] H. B. Shin, J. G. Park, S. K. Chung, H. W. Lee, and T. A. Lipo, "Generalized steady-state analysis of multiphase interleaved boost converter with coupled inductors," *IEE Proc. Electron. Power Appl.*, vol. 152, no. 3, pp. 584–594, May 2005.

[17] W. Wen and Y. S. Lee, "A two-channel interleave boost converter with reduced core loss and copper loss," in *Proc. IEEE Power Electron. Spec. Conf.*, 2004, pp. 1003–1009.

[18] E. Labouré, A. Cunière, T. A. Meynard, F. Forest, and E. Sarraute, "A theoretical approach to intercell transformers, application to interleaved converters," *IEEE Trans. Power Electron.*, vol. 23, no. 1, pp. 464–473, Jan. 2008.

[19] H. Kosai, S. Mcneal, B. Jordan, J. Scofield, B. Ray, and Z. Turgut, "Coupled inductor characterization for a high performance interleaved boost converter," *IEEE Trans. Magn.*, vol. 45, no. 10, pp. 4812–4815, Oct. 2009.

[20] F. Zheng, Y. Pei, Y. Liu, L. Wang, X. Yang, and Z. Wang, "Design coupled inductors for interleaved converters using a three leg core," *IEEE Trans. Magn.*, vol. 44, no. 12, pp. 4697–4705, Dec. 2009.

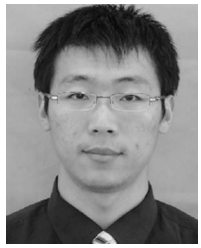

Fei Yang (S'10) was born in Shanxi, China, in 1983. He received the B.S. degree in electrical engineering and automatization from the Nanjing University of Aeronautics and Astronautics, Nanjing, China, in 2006, where he is currently working toward the Ph.D. degree in electrical engineering.

His main research interests include PFC converters, EMI filter design, and dc/dc converters.

Xinbo Ruan (M'97–SM'02) was born in Hubei, China, in 1970. He received the B.S. and Ph.D. degrees in electrical engineering from Nanjing University of Aeronautics and Astronautics (NUAA), Nanjing, China, in 1991 and 1996, respectively.

In 1996, he joined the Faculty of Electrical Engineering Teaching and Research Division, NUAA, and became a Professor in 2002 at the College of Automation Engineering, NUAA, where he has been engaged in teaching and research in the field of power electronics. From August to October 2007, he was a Research Fellow in the Department of Electronics and Information Engineering, Hong Kong Polytechnic University, Kowloon, Hong Kong. Since March 2008, he has been with the College of Electrical and Electronic Engineering, Huazhong University of Science and Technology, Wuhan, China. He has published more than 100 technical papers in journals and conferences and also published three books. He is a Guest Professor at Beijing Jiaotong University, Beijing, China, and Hefei University of Technology, Hefei China. His main research interests include soft-switching dc/dc converters, soft-switching inverters, power factor correction converters, modeling the converters, power electronics system integration and renewable energy generation system.

Dr. Ruan was awarded the Delta Scholar by the Delta Environment and Education Fund in 2003, and was awarded the Special Appointed Professor of the Chang Jiang Scholars Program, by the Ministry of Education, China, in 2007. From 2005, he has served as Vice President of the China Power Supply Society, and since 2008, he has been a member of the Technical Committee on Renewable Energy Systems within the IEEE Industrial Electronics Society. He is a Senior Member of the IEEE Power Electronics Society and the IEEE Industrial Electronics Society.

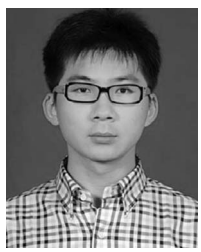

Yang Yang was born in Shaanxi, China, in 1988. He received the B.S. degree in electrical engineering and automatization from Nanjing University of Aeronautics and Astronautics (NUAA), Nanjing, China, in 2010, where he is currently working toward the M.S. degree in electrical engineering.

His main research interests include dc/dc converters, ac/dc converters, and power supplies for LED.

Zhihong Ye (M'00) was born in Zhejiang, China, in 1969. He received the B.S. and M.S. degrees in electrical engineering from Tsinghua University, Beijing, China, in 1992 and 1994, respectively. He received the Ph.D. degree from the Bradley Department of Electrical and Computing Engineering, Virginia Polytechnic Institute and State University, Blacksburg, VA, in 2000.

From 2000 to 2005, he was with General Electric Global Research Center, Niskayuna, NY, as an Electrical Engineer. From 2005 to 2006, he was with Dell as a Commodity Quality Manager. Since 2006, he has been with the LiteOn Technology Corporation, Nanjing, China, as the Director of Research and Development. He holds seven U.S. patents, and has published more than 30 technical papers in transactions and international conferences. His research interests include high density, high efficiency power supply for computing, communication and consumer electronics applications, digital control, power converter topologies and controls, and soft-switching techniques.